IEEE Access
Multidisciplinary | Rapid Review | Open Access Journal

Received February 28, 2022, accepted March 9, 2022, date of publication March 11, 2022, date of current version March 21, 2022.

Digital Object Identifier 10.1109/ACCESS.2022.3158984

Bandpass Filter and Diplexer Based on Dual-Mode Dielectric Filled Waveguide Resonators

WEI QIN, (Member, IEEE), JIANG LIU, HAI-LING ZHANG, WEN-WEN YANG, (Member, IEEE), AND JIAN-XIN CHEN, (Senior Member, IEEE)
School of Information Science and Technology, Nantong University, Nantong 226019, China

Corresponding author: Jian-Xin Chen (jjxchen@hotmail.com)

This work was supported in part by the National Natural Science Foundation of China under Grant 61971244; in part by the Natural Science Foundation of Jiangsu Province, China, under Grant BK20201438; and in part by the Qing Lan Project of Jiangsu Province.

ABSTRACT This paper presents the designs of a bandpass filter (BPF) and a diplexer based on the TM_{210} mode and the TM_{120} mode of the dielectric filled waveguide resonators (DFWRs). The DFWR is designed by integrating a dielectric main body and a printed circuit board (PCB) cover. The PCB cover is electrically connected with the top surface of the dielectric body. For each mode, metallized blind holes can be set at its maximum electric-field points to excite or extract it and the other mode will not be influenced. Microstrip lines on the PCB are utilized to connect different pairs of the metallized blind holes to form the internal and external coupling structures. For verification, a BPF and a diplexer are designed, fabricated and measured based on the DFWRs. In measurement, the BPF is with a frequency band of 2.515 GHz - 2.675 GHz, an insertion loss of 0.6 dB, and a return loss of 20 dB. The two frequency bands of the proposed diplexer are 3.3 GHz - 3.4 GHz and 3.7 GHz - 3.8 GHz. For the two frequency bands, the measured insertion losses are 0.9 dB/0.85 dB and the isolations are better than 40 dB/50 dB.

INDEX TERMS Dielectric filled waveguide resonator (DFWR), printed circuit board (PCB), dual-mode, bandpass filter, diplexer.

I. INTRODUCTION

Bandpass filter (BPF) is always one of the essential and crucial components in the wireless communication systems [1]–[5]. No matter what technology is used, miniaturization is an eternal topic in the BPF designs. Since the utilization of the dual-mode resonators could reduce the filter size to a half, it has been an effective and popular method to realize miniaturization. In recent years, many single-band BPFs based on different kinds of dual-mode resonators have been reported [6]–[15]. In [6], three identical quasi-lumped structures were loaded at a microstrip ring to form a dual-mode resonator, which is used to design a second-order BPF. Similarly, a dual-mode resonator was constructed by loading four step-impedance stubs at a microstrip ring and the use of the step-impedance stubs makes the implemented BPF with wide stopband performance [7]. The stub-loaded half-wavelength microstrip resonators also feature the dual-mode characteristics and have been widely utilized to design BPFs with compact sizes [8]–[10]. Although the above dual-mode resonators based on the microstrip technology merit compact size and light weight, their low quality factors usually make the designed BPFs with high losses. The dual-mode resonators with high quality factors have been proposed to design the BPFs featuring extremely low loss, such as the metal waveguide cavity (MWC) [11], [12] and the dielectric resonator (DR) [13]–[16]. However, these two kinds of resonators are heavy due to the employment of the metal cavities. For the applications in the 5G communication systems, the BPF is required to own a low loss and a light weight at the same time. Accordingly, the microstrip resonators, the MWCs and the DRs can no longer fulfil the requirements of the 5G applications. Dielectric filled waveguide resonator (DFWR) emerges as the most promising selection because of its merits of low loss and light weight [17]. Therefore, it is necessary and crucial to proposed dual-mode DFWRs to design miniaturized single-band BPFs.

The associate editor coordinating the review of this manuscript and approving it for publication was Qi Luo.

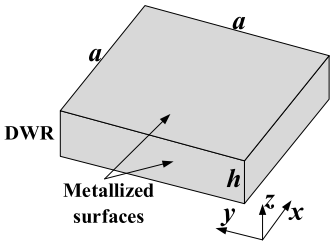

FIGURE 1. 3D view of the square DWR.

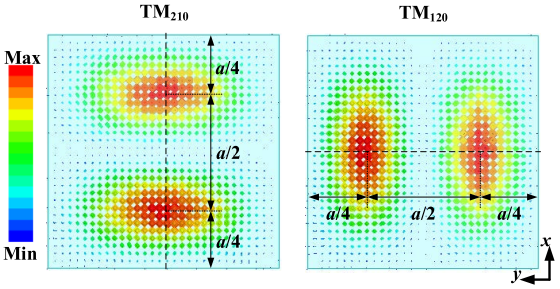

FIGURE 2. Electric-field distributions of the TM210 and TM120 modes of the square DWR.

Diplexer, which is also crucial in wireless communication systems, is usually composed of two BPFs with different working frequency bands. The diplexers based on different kinds of dual-mode or triple-mode resonators have been reported [18]–[25]. In [18], the dual-mode microstrip ring resonators were applied to design a diplexer with two close channels, where an open-ended stub was used to realize the impedance matching. One stub-loaded microstrip resonator could be used to split the signals to two different channels constructed by the resonators with different resonant frequencies, forming diplexers without extra matching circuits [19]–[21]. This idea was recently applied to designing the coaxial diplexers with the characteristics of low loss and high isolation [22]. Other dual-mode resonator with high quality factors, such as the MWC [23] and the DR [24], were also utilized to design the low-loss diplexers. Similar to the BPFs, the microstrip diplexers own high losses, while the diplexers by using the coaxial resonators, the MWCs or the DRs were heavy. Therefore, it is also important to design light and low-loss diplexers by using the promising DFWRs.

In this paper, the TM_{210} mode and the TM_{120} mode of the DFWR is studied and applied to the BPF and diplexer designs. According to the electromagnetic field distribution of the two modes, metallized blind holes are set at the maximum electric-field points of each mode to excite or extract the corresponding mode without influencing the other mode. A printed circuit board (PCB) is electrically connected with the top surface of the dielectric body, forming the DFWR. The microstrip lines on the PCB connect the metallized blind holes so that different types of coupling structures are constructed. For a square DFWR, the two modes are degenerate and an internal coupling structure between them is proposed for the dual-mode BPF designs. A fourth-order BPF is designed with a frequency band of 2.515 GHz - 2.675 GHz by using only two square DFWRs. For a rectangular DFWR, the two modes are separated from each other and utilized to design a diplexer, whose two frequency bands are 3.3 GHz - 3.4 GHz and 3.7 GHz - 3.8 GHz, respectively. The designed BPF and diplexer are fabricated and measured for verification. For the BPF, an in-band insertion loss of 0.6 dB and an in-band return loss better than 20 dB are obtained. Its size is about 30% smaller than the BPF using the fundamental mode. For the diplexer, the measured insertion losses are around 0.9 dB and the isolations are better than 40 dB for both frequency bands.

II. BPF BASED ON DUAL-MODE SQUARE DFWRS

A. MODE ANALYSIS

The DFWRs can be in various shapes, such as square, rectangle, circle and so on. Fig. 1 shows the diagram of the square DFWR. The dielectric material of the DFWR is with a relative permittivity of 20.3 and a loss tangent of 1.5×10^{-4}. The outer surfaces of the DFWR are metallized by plating silver. The TM_{210} mode and the TM_{120} mode are found to be degenerate and closest to the fundamental TM_{110} mode. If the edge a of the square DFWR is 26 mm, the resonant frequency of the TM_{110} mode is about 1.8GHz, while the resonant frequencies of the TM_{210} mode and the TM_{120} mode are around 2.6 GHz. It means that a dual-mode DFWR employing the TM_{210} mode and the TM_{120} mode is about 30% smaller than two single-mode DFWRs using the TM_{110} mode. For a given order, therefore, the BPF using the proposed dual-mode DFWR will be about 30% smaller than that using the single-mode DFWR. The electric-field distributions of the TM_{210} mode and the TM_{120} mode are shown in Fig. 2. It can be seen that the two maximum electric-field points of each mode are located at the quarter and three-quarter positions along the center line. Besides, the maximum electric-field points of the TM_{210} mode correspond to the nearly-minimum electric-field points of the TM_{120} mode and vice versa. The metallized blind holes can be set at the maximum electric-field points to independently excite or extract the two modes. As shown in Fig. 3, the positions namely A1 and A2 are for the TM_{210} mode, while those named as B1 and B2 are for the TM_{120} mode.

B. COUPLING STRUCTURES

Based on the above-mentioned metallized blind holes, two coupling structures, i.e. the internal coupling structure between the two modes of a single DFWR and the external coupling structure between two adjacent DFWRs, are proposed for the BPF designs.

As shown in Fig. 4, a piece of PCB is stacked on the DFWR and they are electrically connected by soldering. The substrate of the PCB is the Rogers 4003C with a relative permittivity of 3.55 and a thickness of 0.813 mm. Two metallized blind holes are set on the top surface of the DFWRs A length of microstrip line connects the two metallized blind holes, providing an internal coupling path between the TM_{210} mode

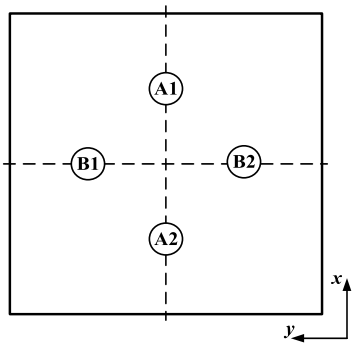

FIGURE 3. Locations of the blind holes for the two modes.

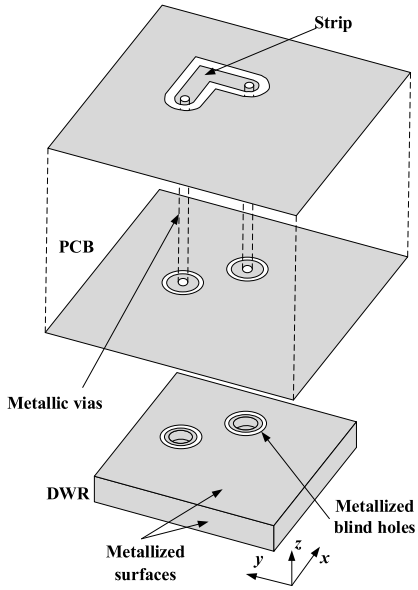

FIGURE 4. Internal coupling structure between the two modes.

and the TM_{120} mode of the DFWR. This internal coupling is related not only to the width of the microstrip line but also to the depth of the metallized blind holes.

The external coupling structure between two adjacent DFWRs are exhibited in Fig. 5. It is also realized by utilizing a length of microstrip line to connect two metallized blind holes for the TM_{120} mode. Similarly, the width of the microstrip line and the depth of the metallized blind holes will also be the main parameters those control the external coupling.

C. DUAL-MODE BPF DESIGN

A fourth-order BPF is constructed by two dual-mode DFWRs, as shown in Fig. 6. In Fig. 6, kh_1, kh_2, kh_3 and kh_4 are the depths of the corresponding metallized blind holes, while cx_1, cx_2, cy_1 and cy_2 define their positions. Its working principle is described as follows. Firstly, the TM_{210} mode will be excited in the DFWR 1 through Port 1. Secondly, the TM_{210} mode will be coupled to the TM_{120} mode by the internal coupling structure. Thirdly, the TM_{120} mode will be coupled from DFWR 1 to DFWR 2 through the external

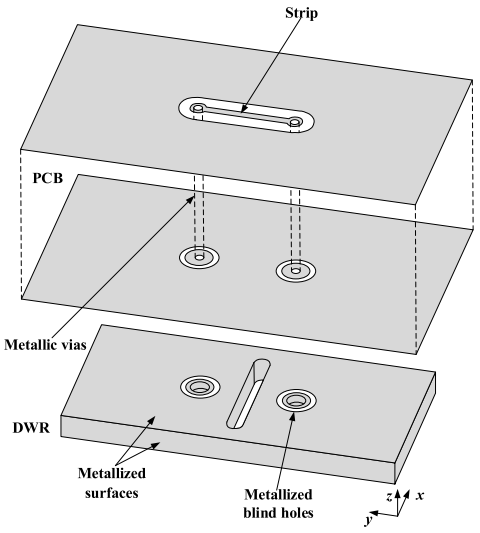

FIGURE 5. External coupling structure between two adjacent DWRs.

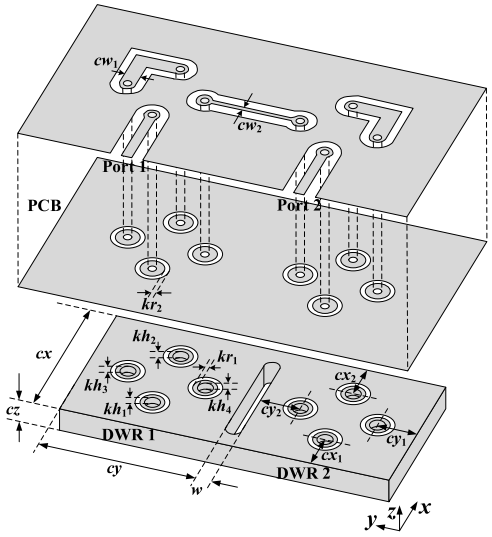

FIGURE 6. 3D view and physical parameters of the dual-mode DWR bandpass filter.

coupling structure. Then, in DFWR 2, the TM_{120} mode will be coupled to the TM_{210} mode by the internal coupling structure. Finally, the TM_{210} mode will be extracted from the DFWR 2 through Port 2. Accordingly, the coupling route of the proposed fourth-order BPF is as shown in Fig. 7. The M_{SL} in Fig. 7 represents the source-to-load coupling that is caused by the parallel microstrip lines at the two ports. This coupling is much smaller than the main couplings. Therefore, it will generate two transmission zeros far away from the passband and will only slightly influence the passband performance. Moreover, the simulated un-loaded quality factor of the DFWR is about 1200, which is large enough to obtain low insertion loss.

The target BPF is required to own a center frequency of 2.594 GHz, a fractional bandwidth (*FBW*) of about 6%, and an in-band return loss of 20 dB. According to the coupled

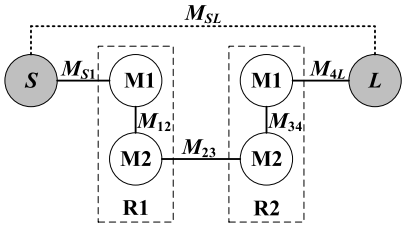

FIGURE 7. Coupling route of the dual-mode DWR bandpass filter.

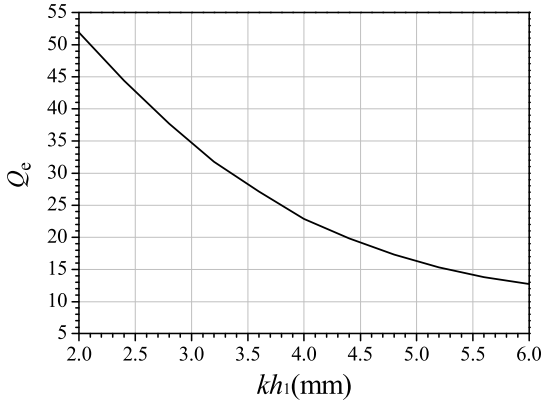

FIGURE 8. The relationship between Q_e and kh_1.

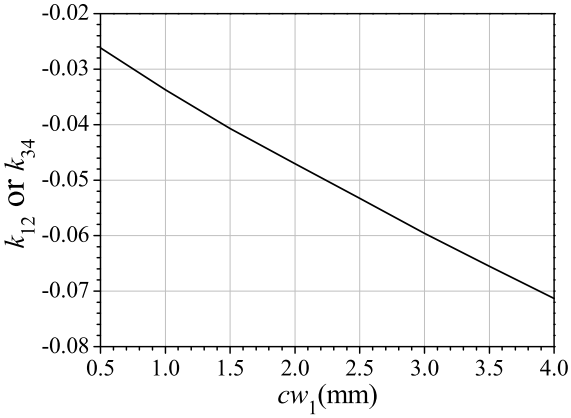

FIGURE 9. The relationship between the internal coupling and cw_1.

resonator theory [26], the following steps could be conducted to design the target BPF.

1. Based on the specifications of the BPF, the normalized coupling matrix can be synthesized as

$$[M] = \begin{array}{c} \\ S \\ 1 \\ 2 \\ 3 \\ 4 \\ L \end{array} \begin{array}{c} \begin{array}{cccccc} S & 1 & 2 & 3 & 4 & L \end{array} \\ \begin{bmatrix} 0 & 1.03 & 0 & 0 & 0 & 0.003 \\ 1.03 & 0 & -0.9 & 0 & 0 & 0 \\ 0 & -0.9 & 0 & -0.7 & 0 & 0 \\ 0 & 0 & -0.7 & 0 & -0.9 & 0 \\ 0 & 0 & 0 & -0.9 & 0 & 1.03 \\ 0.003 & 0 & 0 & 0 & 1.03 & 0 \end{bmatrix} \end{array}, \quad (1)$$

where the negative values represent the capacitive couplings and the positive values are the inductive couplings.

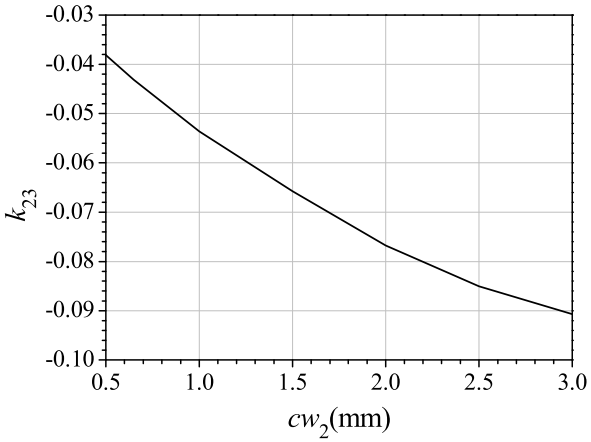

FIGURE 10. The relationship between the external coupling and cw_2.

TABLE 1. Physical parameters of the Optimized BPF (Unit: mm).

cx	cy	cz	w	kh_1	kh_2	kh_3	kh_4	kr_1
26	26	7.2	2.6	5.2	5.2	5.2	5.2	1.2
kr_2	cx_1	cx_2	cy_1	cy_2	cw_1	cw_2	w_{50}	
0.6	6.5	6.5	6.5	6.5	2.65	0.65	1.75	

2. According to (1), the external quality factor (Q_e) and the couplings can be calculated to be

$$Q_e = \frac{1}{M_{s1}^2 \cdot FBW} = 15.32 \quad (2)$$

and

$$\begin{aligned} k_{12} &= k_{34} = M_{12} \cdot FBW = -0.0554 \\ k_{23} &= M_{23} \cdot FBW = -0.0431 \\ k_{SL} &= M_{SL} \cdot FBW = 0.00018. \end{aligned} \quad (3)$$

3. To determine the desired Q_e and coupling coefficients, they are extracted for the corresponding physical parameters. The Q_e changes after the depth (kh_1) of the metallized blind hole for feeding, as plotted in Fig. 8.

4. Based on Fig. 8, kh_1 is defined to be 5.2 mm to obtain the desired Q_e in (2). To maintain the symmetry of the DFWR, kh_2, kh_3 and kh_4 are all fixed to be 5.2 mm for simplification.

5. Fig. 9 and Fig. 10 indicate that both the internal and external couplings vary after the widths of the connecting microstrip line. Accordingly, c_{w1} and c_{w2} can be determined to be 2.6 mm and 0.65 mm so that the desired main coupling coefficients in (3) can be realized, respectively. Because the source-to-load coupling is much smaller than the main couplings, it is not considered in the design.

6. The fourth-order BPF is constructed and simulated in the ANSYS Electromagnetic Simulator. After a simple fine-tuning process, the optimized physical parameters are attained and listed in Table 1. The simulated and synthesized results are shown in Fig. 11, in which good agreements are observed.

In simulation, the boundary conditions of the proposed BPF are set to be as consistent with the practical boundary

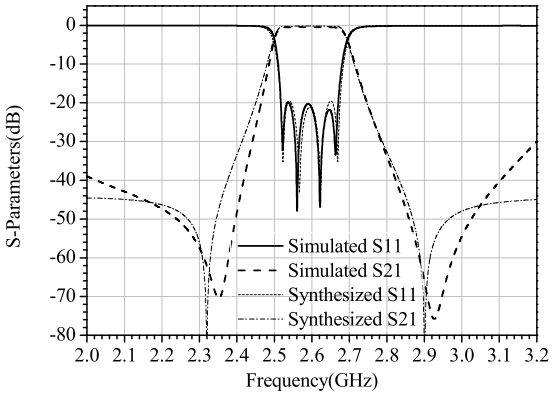

FIGURE 11. Synthesized and simulated results of the dual-mode DWR BPF.

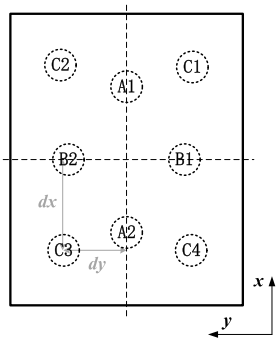

FIGURE 12. Locations of the blind holes for the two modes.

conditions as possible. The metal surfaces of the DFWRs are set to be silver. The metal surface of the PCB is set as cooper. An air-filled radiation boundary condition, which is also known as an absorbing boundary condition, is set at the top of the PCB.

III. DIPLEXER BASED ON RECTANGULAR DFWRS

The TM_{210} mode and the TM_{120} mode of the square DFWR used in the last section have the same resonant frequencies. If the DFWR becomes rectangular, the two modes will split from each other. In this section, the rectangular DFWR will be applied to the diplexer design.

The electric-field distributions of the TM_{210} mode and the TM_{120} mode of the rectangular DFWR are similar with those of the square DFWR. The difference is that the resonant frequencies of the two modes are split due to the change of the dimensions. As shown in Fig. 12, the positions A1 and A2 are for the TM_{210} mode, while those identified as B1 and B2 are for the TM_{120} mode. For a diplexer, there should be a common port that can excite both modes to support the two channels. A metallized blind hole at the positions C1, C2, C3 or C4 could achieve this function.

The proposed DFWR diplexer is shown in Fig. 13, where five DFWRs are employed. Among them, DFWR 1 is shared by the two channels. To excite both the TM_{210} mode and TM_{120} mode of shared DFWR 1, a metallized blind hole should be set at the positions C1, C2, C3 or C4 in Fig. 12.

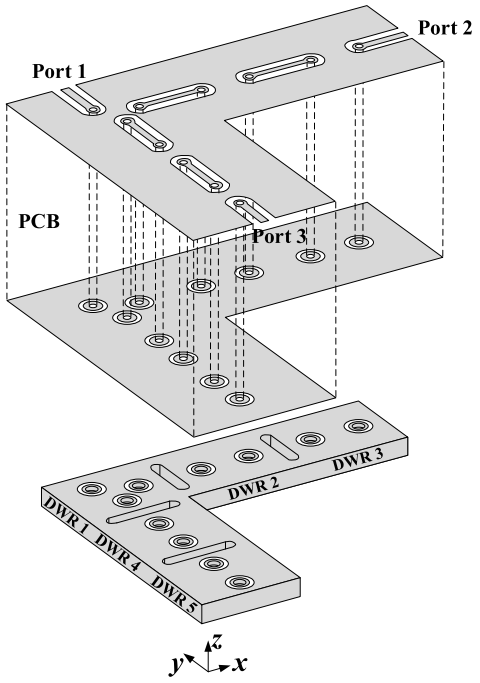

FIGURE 13. 3D view of the proposed DWR diplexer.

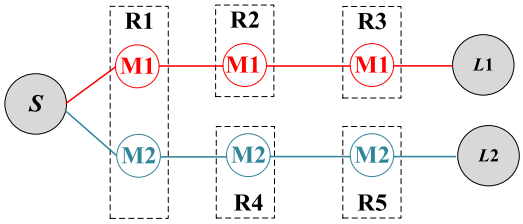

FIGURE 14. Coupling topology of the proposed DWR diplexer.

DFWR 2 and DFWR 3 are to support one channel, while DFWR 4 and DFWR 5 are to support the other channel. Its coupling topology is given in Fig. 14. The design process of the diplexer is similar to that of the BPF. The main difference lies in the control of the Q_es for the TM_{210} mode and the TM_{120} mode of the common DFWR. The extracted Q_es for both modes are plotted in Fig. 15, where the position parameters dx and dy are defined in Fig. 12. The depth of the corresponding metallized blind hole is fixed in the extraction. For the TM_{210} mode, the Q_e enlarges when dy increases and reduces when dx increases. For the TM_{120} mode, the Q_e almost remains unchanged when dy changes but enlarges when dx increases. Therefore, the Q_es for the two modes can be controlled independently. Moreover, the depth of the metallized blind hole could also be an alternative of adjusting the Q_es for both modes.

A third-order diplexer with two frequency bands of 3.3 GHz - 3.4 GHz and 3.7 GHz - 3.8 GHz is designed. Fig. 16 plots the simulated and synthesized results of the designed diplexer. As it can be seen, the isolation of the upper channel is about 45 dB, which can be improved by generating a transmission zero. As shown in Fig. 17, two microstrip lines attached at the microstrip lines in the coupling structure are

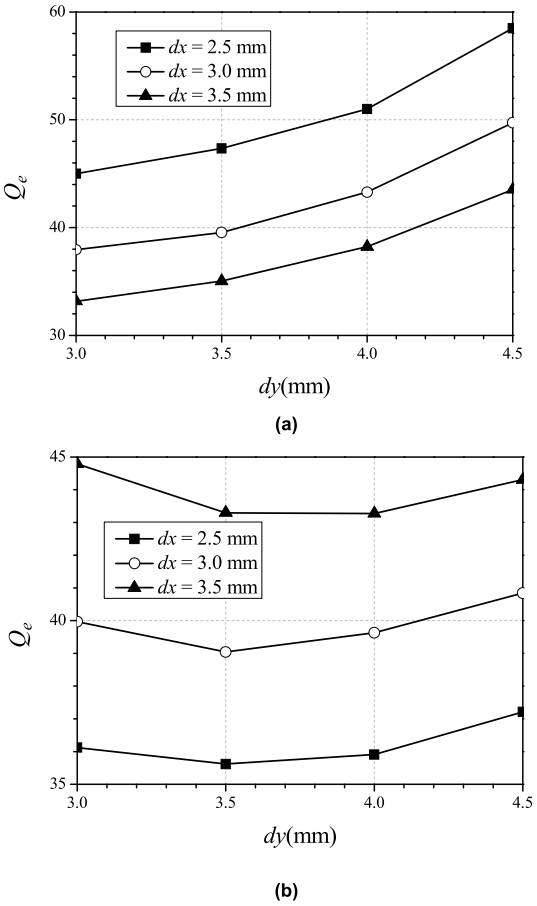

FIGURE 15. The extracted Q_es for (a) the TM_{210} mode and (b) the TM_{210} mode for the common DWR.

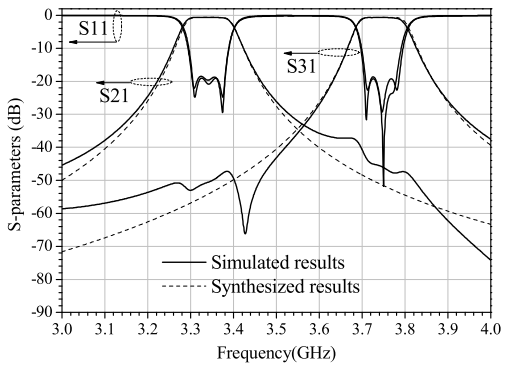

FIGURE 16. Synthesized and simulated results of the DWR diplexer.

employed. As a result, the isolation of the upper channel is improved to be better than 60 dB, as shown in Fig. 18.

IV. MEASUREMENT AND DISCUSSION

For verification, the designed BPF and diplexer are fabricated, assembled and measured. The measurement is conducted by the Agilent N5230C vector network analyzer. Fig. 19 shows the photographs of the fabricated fourth-order BPF. The measured and simulated results are shown in Fig. 20, where good accordance is observed. In measurement, the working frequency band is from 2.515 GHz to 2.675 GHz.

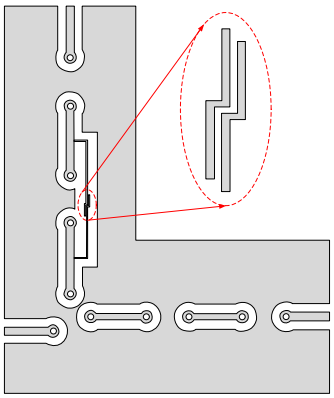

FIGURE 17. Schematic diagram of the structure for introducing transmission zero.

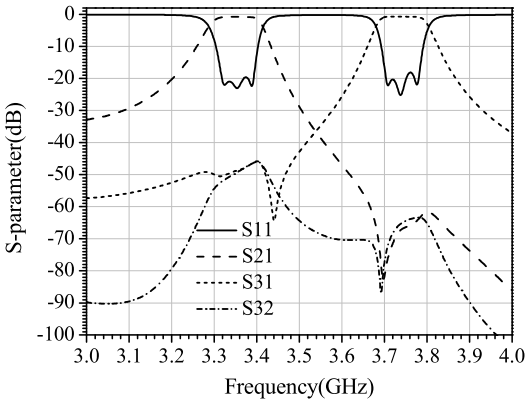

FIGURE 18. Simulated results of the improved DWR diplexer.

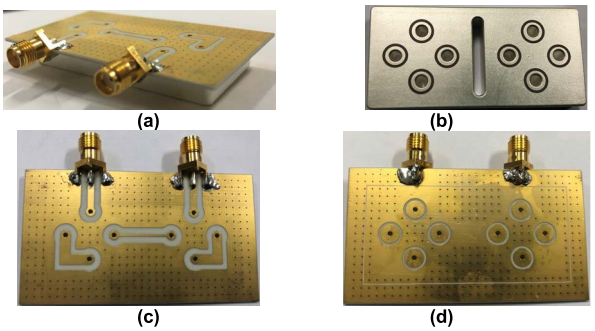

FIGURE 19. Photographs of the fabricated dual-mode DWR BPF: (a) the assembled BPF, (b) the dielectric part, (c) top view of the PCB, and (d) bottom view of the PCB.

The in-band insertion loss is around 0.6 dB and the in-band return loss is better than 20 dB. The comparisons of the proposed dual-mode BPF with previous prototypes are outlined in Table 2. As compared with the reported PCB dual-mode BPFs, the proposed one features much smaller in-band insertion loss and better in-band return loss. Although the in-band insertion loss of the proposed BPF is at the same level as the MWC or DR ones, it features lighter weight and compacter size because no metal cavity is employed. In a word, the proposed BPF using dual-mode DFWRs features a small insertion loss, a light weight and a medium size simultaneously.

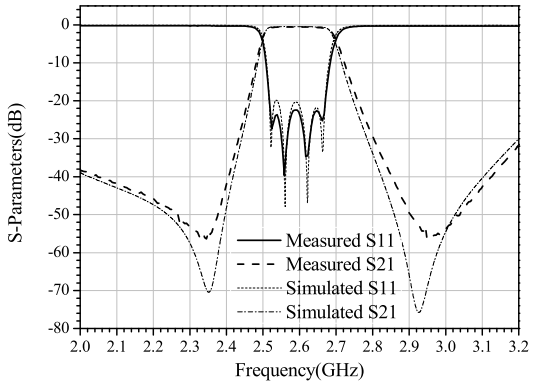

FIGURE 20. Simulated and measured results of the fabricated dual-mode DWR BPF.

TABLE 2. Comparisons with previous dual-mode BPFs.

Ref.	Type	Filter Order	FBW (%)	IL (dB)	RL (dB)	Weight	Size
[6]	PCB	2	4.7	2.5	15	Light	Small
[7]	PCB	2	1.6	2.5	15	Light	Small
[8]	PCB	4	21.1	1.1	15	Light	Small
[10]	PCB	3	13.2	1.2	10	Light	Small
[11]	MWC	4	1.5	0.6	15	Heavy	Large
[12]	MWC	4	0.12	0.71	25	Heavy	Large
[14]	DR	2	0.39	0.3	22	Heavy	Large
[15]	DR	2	1.2	0.8	11.5	Heavy	Large
This work	DWR	4	6	0.6	23	Medium	Medium

IL: insertion loss; RL: return loss

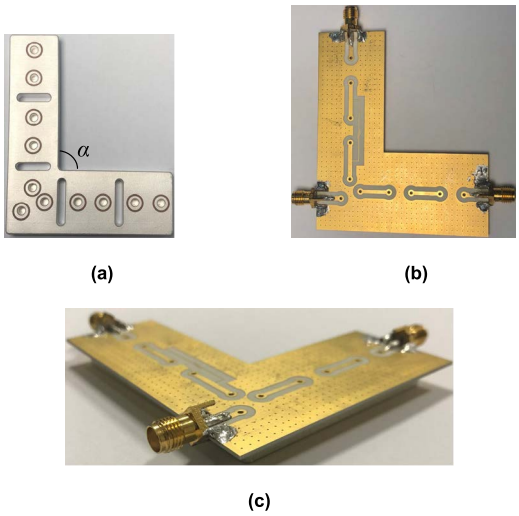

FIGURE 21. Photographs of the fabricated DWR diplexer: (a) Top view of the dielectric part, (b) top view of the PCB, and (c) the assembled diplexer.

The photographs of the fabricated DFWR diplexer are given in Fig. 21. Fig. 22 plots its measured and simulated results. In measurement, the frequency bands of the two channels are 3.3 GHz - 3.4 GHz and 3.7 GHz - 3.8 GHz, respectively. The measured insertion losses in the two channels are found to be 0.9 dB and 0.85 dB. The measured isolations are 40 dB and 50 dB for the lower and upper channels, respectively. Discrepancies between the simulated

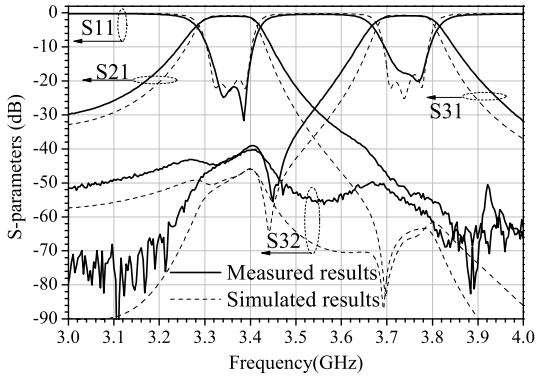

FIGURE 22. Simulated and measured results of the fabricated DWR diplexer.

TABLE 3. Comparisons with previous diplexers.

Ref.	Type	FBW (%)	IL (dB)	ISO (dB)	Weight
[17]	PCB	5/5	2.1/2.1	24/24	Light
[18]	PCB	3.1/2.8	1.22/1.46	37/36	Light
[19]	PCB	3.6/3.3	1.2/1.5	40/35	Light
[20]	PCB	6.7/3.6	1.46/2.15	38/38	Light
[21]	CR	16/6	0.72/0.55	50/60	Heavy
[23]	DR	0.85/1.1	0.8/0.5	35/33	Heavy
This work	DWR	3/2.7	0.9/0.85	40/50	Medium

ISO: isolation

and measured results are observed. It is mainly because that the angle α in Fig. 21(a) is slightly bigger than 90°. The performance of the proposed DFWR diplexer is compared with the reported diplexers in Table 3. It can be summarized that the proposed diplexer owns a low insertion loss and a light weight at the same time since the DFWR technology is used. Besides, its isolations are also excellent for many practical applications.

V. CONCLUSION

In this paper, the TM_{210} mode and the TM_{120} mode of the DFWRs are investigated. Metallized blind holes are set at the maximum electric-field points of the two modes so that each mode can be excited or extracted independently. A dual-mode BPF is realized by using the square DFWRs, where the number of the resonators used can be reduce by half. Besides, the rectangular DFWRs are utilized to design a diplexer. Both the proposed BPF and diplexer own a low loss and a light weight simultaneously, making them the promising candidates for the basestation applications in the 5G and future wireless communication systems.

REFERENCES

[1] G.-Z. Liang and F.-C. Chen, "A compact dual-wideband bandpass filter based on open-/short-circuited stubs," *IEEE Access*, vol. 8, pp. 20488–20492, 2020.
[2] L. Gao, T.-W. Lin, and G. M. Rebeiz, "Design of tunable multi-pole multi-zero bandpass filters and diplexer with high selectivity and isolation," *IEEE Trans. Circuits Syst. I, Reg. Papers*, vol. 66, no. 10, pp. 3831–3842, Oct. 2019.
[3] G. Shen, W. Che, and Q. Xue, "Compact microwave and millimeter-wave bandpass filters using LTCC-based hybrid lumped and distributed resonators," *IEEE Access*, vol. 7, pp. 104797–104809, 2019.

[4] C. H. Kim and K. Chang, "Wide-stopband bandpass filters using asymmetric stepped-impedance resonators," *IEEE Microw. Wireless Compon. Lett.*, vol. 23, no. 2, pp. 69–71, Feb. 2013.
[5] W. Qin and Q. Xue, "Complementary compact microstrip resonant cell and its applications to microwave single- and dual-band bandpass filters," *IEEE Trans. Microw. Theory Techn.*, vol. 61, no. 2, pp. 773–781, Feb. 2013.
[6] H.-W. Hsu, C.-H. Lai, and T.-G. Ma, "A miniaturized dual-mode ring bandpass filter," *IEEE Microw. Wireless Compon. Lett.*, vol. 20, no. 10, pp. 542–544, Oct. 2010.
[7] J. Wang, J.-L. Li, J. Ni, S. Zhao, W. Wu, and D. Fang, "Design of miniaturized microstrip dual-mode filter with source-load coupling," *IEEE Microw. Wireless Compon. Lett.*, vol. 20, no. 6, pp. 319–321, Jun. 2010.
[8] L. Gao, X. Y. Zhang, B.-J. Hu, and Q. Xue, "Novel multi-stub loaded resonators and their applications to various bandpass filters," *IEEE Trans. Microw. Theory Techn.*, vol. 62, no. 5, pp. 1162–1172, May 2014.
[9] H. Xu, J. Wang, L. Zhu, F. Huang, and W. Wu, "Design of a dual-mode balun bandpass filter with high selectivity," *IEEE Microw. Wireless Compon. Lett.*, vol. 28, no. 1, pp. 22–24, Jan. 2018.
[10] M. Zhou, X. Tang, and F. Xiao, "Miniature microstrip bandpass filter using resonator-embedded dual-mode resonator based on source-load coupling," *IEEE Microw. Wireless Compon. Lett.*, vol. 20, no. 3, pp. 139–141, Mar. 2010.
[11] C. Tomassoni, S. Bastioli, and R. Sorrentino, "Generalized TM dual-mode cavity filters," *IEEE Trans. Microw. Theory Techn.*, vol. 59, no. 12, pp. 3338–3346, Dec. 2011.
[12] M. Guglielmi, P. Jarry, E. Kerherve, O. Roquebrun, and D. Schmitt, "A new family of all-inductive dual-mode filters," *IEEE Trans. Microw. Theory Techn.*, vol. 49, no. 10, pp. 1764–1769, Oct. 2001.
[13] J.-X. Chen, Y.-L. Li, W.-W. Yang, and Z.-H. Bao, "Design of compact bandpass filters using novel dual-mode dielectric patch resonator," *IEEE Access*, vol. 6, pp. 18705–18712, 2018.
[14] M. Hoft, "Y-shape dielectric dual-mode resonator," *IEEE Trans. Microw. Theory Techn.*, vol. 56, no. 12, pp. 3066–3071, Dec. 2008.
[15] J.-X. Chen, J. Li, W. Qin, J. Shi, and Z.-H. Bao, "Design of balanced and balun filters using dual-mode cross-shaped dielectric resonators," *IEEE Trans. Microw. Theory Techn.*, vol. 65, no. 4, pp. 1226–1234, Apr. 2017.
[16] J. Li, Y. Zhan, W. Qin, Y. L. Wu, and J.-X. Chen, "Differential dielectric resonator filters," *IEEE Trans. Compon., Packag., Manuf. Technol.*, vol. 7, no. 4, pp. 637–645, Apr. 2017.
[17] W. Qin, J. Liu, W.-W. Yang, J.-X. Chen, Y. Li, and R.-L. Xu, "Integrated-designs of filtering circuits based on adjustable dielectric waveguide resonators," *IEEE Trans. Circuits Syst. II: Exp. Briefs*, vol. 69, no. 2, pp. 284–288, Feb. 2022.
[18] H. Peng and Y. Chiang, "Microstrip diplexer constructed with new types of dual-mode ring filters," *IEEE Microw. Wireless Compon. Lett.*, vol. 25, no. 1, pp. 7–9, Jan. 2015.
[19] M.-L. Chuang and M.-T. Wu, "Microstrip diplexer design using common T-shaped resonator," *IEEE Microw. Wireless Compon. Lett.*, vol. 21, no. 11, pp. 583–585, Nov. 2011.
[20] X. Guan, F. Yang, H. Liu, and L. Zhu, "Compact and high-isolation diplexer using dual-mode stub-loaded resonators," *IEEE Microw. Wireless Compon. Lett.*, vol. 24, no. 6, pp. 385–387, Jun. 2014.
[21] J.-K. Xiao, M. Zhang, and J.-G. Ma, "A compact and high-isolated multiresonator-coupled diplexer," *IEEE Microw. Wireless Compon. Lett.*, vol. 28, no. 11, pp. 999–1001, Nov. 2018.
[22] Y. Xie, F.-C. Chen, Q.-X. Chu, and Q. Xue, "Dual-band coaxial filter and diplexer using stub-loaded resonators," *IEEE Trans. Microw. Theory Techn.*, vol. 68, no. 7, pp. 2691–2700, Jul. 2020.
[23] T. V. Duong, W. Hong, Z. C. Hao, W. C. Huang, J. X. Zhuang, and V. P. Vo, "A millimeter wave high-isolation diplexer using selectivity-improved dual-mode filters," *IEEE Microw. Wireless Compon. Lett.*, vol. 26, no. 2, pp. 104–106, Feb. 2016.
[24] L. Xu, W. Yu, and J.-X. Chen, "Unbalanced-/balanced-to-unbalanced diplexer based on dual-mode dielectric resonator," *IEEE Access*, vol. 9, pp. 53326–53332, 2021.
[25] Z.-C. Zhang, Q.-X. Chu, S.-W. Wong, S.-F. Feng, L. Zhu, Q.-T. Huang, and F.-C. Chen, "Triple-mode dielectric-loaded cylindrical cavity diplexer using novel packaging technique for LTE base-station applications," *IEEE Trans. Compon., Packag., Manuf. Technol.*, vol. 6, no. 3, pp. 383–389, Mar. 2016.
[26] J.-S. Hong and M. J. Lancaster, *Microstrip Filters for RF/Microwave Applications*, 2nd ed. Hoboken, NJ, USA: Wiley, 2011.

WEI QIN (Member, IEEE) was born in Jiangsu, China. He received the B.Sc. degree in electronic engineering and the M.Sc. degree in electromagnetic fields and microwave technology from Southeast University, Nanjing, China, in 2007 and 2010, respectively, and the Ph.D. degree in electronic engineering from the City University of Hong Kong, Hong Kong, China, in 2013.

From July 2013 to November 2013, he was a Senior Research Associate with the State Key Laboratory of Millimeter Waves (HK), City University of Hong Kong. Since 2014, he has been with the School of Electronics and Information, Nantong University, Nantong, Jiangsu, where he is currently a Professor. His research interests include deign and application of microwave devices and antennas.

JIANG LIU was born in Jiangsu, China. He received the M.Sc. degree in electromagnetic field and microwave technology from Nantong University, Nantong, China.

His research interests include microwave circuits and antennas.

HAI-LING ZHANG was born in Jiangsu, China. She is currently pursuing the M.Sc. degree in electromagnetic field and microwave technology from Nantong University, Nantong, China.

Her research interests include microwave circuits and antennas.

WEN-WEN YANG (Member, IEEE) received the B.Eng. degree in information engineering and the M.Eng. and Ph.D. degrees in electrical engineering from Southeast University (SEU), Nanjing, China, in 2007, 2010, and 2015, respectively.

He is currently with the School of Electronics and Information, Nantong University, Nantong, China, as an Associate Professor. His research interests include RF, microwave and millimeter-wave passive devices, active antenna array, and antennas for wireless communication. He serves as a Reviewer for several journals, including IEEE TRANSACTIONS ON ANTENNAS AND PROPAGATION, *IET MAP*, and *IET EL*.

JIAN-XIN CHEN (Senior Member, IEEE) was born in Nantong, China, in 1979. He received the B.S. degree from Huai Yin Teachers College, Jiangsu, China, in 2001, the M.S. degree from the University of Electronic Science and Technology of China (UESTC), Chengdu, China, in 2004, and the Ph.D. degree from the City University of Hong Kong, Hong Kong, in 2008.

Since 2009, he has been with Nantong University, Nantong, where he is currently a Professor. He has authored or coauthored more than 100 international referred journals and conference papers. He holds 15 Chinese patents and three U.S. patents. His research interests include RF/microwave differential circuits and antennas, dielectric resonator (DR) filters, and low temperature co-fired ceramic (LTCC) millimeter-wave circuits and antennas.

Dr. Chen received the Best Paper Award Presented at the Chinese National Microwave and Millimeter-Wave Symposium, Ningbo, China, in 2007. He was the Supervisor of the 2014 iWEM Student Innovation Competition Winner, Sapporo, Japan. He was a TPC Co-Chair of IEEE iWEM, in 2016. He has been a Regular Reviewer for several international journals, including four IEEE TRANSACTIONS.